Guidelines for Stability Analysis of the DDSRF-PLL Using LTI and LTP Modelling in the Presence of Imbalance

Beloqui Larumbe, Lucia; Qin, Zian; Bauer, Pavol

DOI
10.1109/OJIES.2022.3178042

Publication date
2022

Document Version
Final published version

Published in
IEEE Open Journal of the Industrial Electronics Society

Citation (APA)
Beloqui Larumbe, L., Qin, Z., & Bauer, P. (2022). Guidelines for Stability Analysis of the DDSRF-PLL Using LTI and LTP Modelling in the Presence of Imbalance. *IEEE Open Journal of the Industrial Electronics Society*, *3*, 339-352. Article 9781849. https://doi.org/10.1109/OJIES.2022.3178042

IEEE Open Journal of the
Industrial Electronics Society

Received 23 March 2022; revised 3 May 2022; accepted 22 May 2022. Date of publication 25 May 2022;
date of current version 13 June 2022. The review of this article was arranged by Associate Editor Eric Monmasson.

Digital Object Identifier 10.1109/OJIES.2022.3178042

Guidelines for Stability Analysis of the DDSRF-PLL Using LTI and LTP Modelling in the Presence of Imbalance

LUCIA BELOQUI LARUMBE (Student Member, IEEE), ZIAN QIN (Senior Member, IEEE), AND PAVOL BAUER (Senior Member, IEEE)

DC Systems, Energy Conversion and Storage Research Group at the Delft University of Technology, 2600AA Delft, The Netherlands

CORRESPONDING AUTHOR: ZIAN QIN (e-mail: z.qin-2@tudelft.nl)

ABSTRACT In this article, the Linear Time Invariant (LTI) and Linear Time Periodic (LTP) models of two different implementations of the DDSRF-PLL in the presence of voltage imbalance are derived analytically. The accuracy of the models is investigated with time domain simulations, frequency scans, and stability analysis. On top of this, a guideline for properly choosing between LTI and LTP models for stability assessment of the DDSRF-PLL according to the degree of grid voltage imbalance is proposed. Furthermore, it is revealed that, depending on the DDSRF-PLL implementation, the positive-sequence voltage might also cause LTP dynamics, rendering the LTI model inaccurate even when the imbalance is low.

INDEX TERMS DDSRF-PLL, Linear Time Periodic, LVRT, small-signal stability, unbalanced system, voltage imbalance.

I. INTRODUCTION

In many applications, power-electronic converters are required to provide Low Voltage Ride Through (LVRT) response. In order to achieve this, it is necessary that the converter keeps synchronism with the grid in the presence of all levels of voltage imbalance. This is especially challenging under weak grid conditions. Consequently, several advanced Phase-Locked Loop (PLL) methods have been developed in the literature [1], like for example, the Decoupled Double Synchronous Reference Frame PLL (DDSRF-PLL) [2]. In order to assess the different stability properties, stability margins, or the parameter design of the PLLs, small-signal models are a common tool for engineers.

Usually, small-signal models are either Linear Time Invariant (LTI) or Linear Time Periodic (LTP). In an LTI system, the state variables are constant (i.e. time invariant) in steady-state, and therefore, linearisation of the system equations can be undertaken around an operating point. Sometimes, systems are naturally LTI, but sometimes, the state variables are forced to be time invariant in steady state using different methods. For example, the system might have an oscillatory steady-state in one reference frame, but if the equations are taken to another frame, then the state variables become constant in steady-state, which allows for LTI linearisation around an operating point. A well-known example is two-level converters in balanced situations with only current control: in the *abc* frame their steady-state is oscillatory, but in the dq frame the steady-state is constant, and therefore in the dq frame an LTI model can be derived. In this case, there is no loss of accuracy in the process since the process is simply a frame transformation [3]. Sometimes, for example with certain converter topologies, more than one dq frame is necessary to force the obtention of an LTI model [4]. Another example of forcing the time-invariance of the system is when the oscillatory behaviour is ignored or considered negligible. For example, in certain systems, grid voltage imbalance or harmonic distortion might induce an oscillatory behaviour in the system equations, so if these elements are ignored, it might be possible to obtain an LTI system. In this case, there is a risk of accuracy loss in the process, since part of the system dynamics are ignored.

In an LTP system, the state variables are oscillatory in steady-state. This means that the state variables are variant in a very specific way: if the variables are in steady-state, their Fourier decomposition needs to lead to harmonic magnitudes

with constant magnitudes and phase-angles. That is to say, there is a steady-state, but it is periodic. In this case, linearisation of the system equations has to be performed around an operating trajectory, instead of an operating point.

Numerous articles have been published about small-signal modelling of PLLs. In the particular case of single-phase PLLs or Frequency-Locked Loops (FLLs), the Linear Time Invariant (LTI) models have been recently challenged, as they are not capable of modelling the double-frequency oscillation typical in these structures. Several articles [5]–[7] have recently shown that the LTI models of different single-phase PLLs or FLLs are not able to predict the stability boundaries for different parameter variations, in comparison to the Linear Time Periodic (LTP) models which perform the task [8]. In order to model more accurately the dynamic effect of certain non-linearities in SOGI-based PLLs/FLLs, [9] proposes also the use of LTP theory. Further, [10] proposes the use of signal-flow graphs for easier understanding of the harmonic propagation in LTP systems, with the application example of single-phase PLLs.

With respect to three-phase PLLs, recent literature shows that LTP modelling might be necessary in the presence of a DC component in the input voltage [11] or in the presence of imbalance [12], [13]. Specifically, [12] focuses on an SRF-PLL and shows that the 100 Hz oscillations that are caused by voltage imbalance in this type of PLL, brings LTP dynamics to the system.[1] When the positive-sequence voltage phase-angle detected by the PLL ($\theta_{\text{PLL+}}$) is fed back within the SRF-PLL, if the negative-sequence voltage (V_{n}) is high enough, the 100 Hz component in the PLL dq signals will inter-modulate with any perturbation $f_{\text{p}}^{\text{dq+}}$ that may be present in the $\theta_{\text{PLL+}}$. This means that, if the voltage has a perturbation at $f_{\text{p}}^{\text{dq+}}$ (defined in the dq frame), the frequencies $f_{\text{p}}^{\text{dq+}}$ and $f_{\text{p}}^{\text{dq+}} \pm 2f_1$ will appear at $\theta_{\text{PLL+}}$ (where f_1 is the fundamental frequency). In turn, these frequencies are part of the signal ($\theta_{\text{PLL+}}$) which is fed back, so inter-modulation happens again and, therefore, in the end, $\theta_{\text{PLL+}}$ will have the frequencies $f_{\text{p}}^{\text{dq+}} \pm 2f_1$, $f_{\text{p}}^{\text{dq+}} \pm 4f_1$, etc. The presence of (infinite) frequency couplings is typical in LTP systems [14].

Both in the case of single-phase or three-phase PLLs in the presence of imbalance, the chosen approach for LTP analysis is usually to develop a Harmonic Transfer Function (HTF) model in the frequency domain (e.g. [5]–[7], [11], [12]). Alternatively, [13] proposes a state-space in the time domain, with which stability can be assessed with the eigenvalues of the monodromy matrix.

One common message in the literature concerning LTP modelling of three-phase PLLs is that LTP models are necessary in the presence of significant imbalance [12], [13]; however, no guidance exists into what level of imbalance constitutes significant enough to justify the use of the LTP method. A comparison of the stability results obtained by the LTP and LTI methods at different imbalance levels (showing the need, or not, to use the LTP method depending on V_{n}) is missing in the literature. Furthermore, the underlying assumption in previous literature is that, when V_{n} is low enough (and the voltage does not present other perturbations), the PLL necessarily behaves as an LTI system. This article shows that this is not always the case. In this article, two different implementations of the DDSRF-PLL are presented and modelled in the presence of voltage imbalance. One of them has significant periodic terms only when V_{n} is high; however, the other has significant LTP dynamics (also) due to the positive-sequence voltage (V_{p}) and, therefore, has significant LTP dynamics even if V_{n} is low, which is a behaviour not predicted by previous literature.

Finally, previous literature assumes that the couplings created by the voltage imbalance must happen at $2f_1$; however, it is shown here that, depending on the specific implementation, the LTP dynamics might appear at $f_{\text{p}}^{\text{dq+}} \pm 2f_1$ (and beyond) or at $f_{\text{p}}^{\text{dq+}} \pm 4f_1$ (and beyond). Thus, this article effectively contributes to the literature of small-signal models of three-phase PLLs.

When designing the PLL, one critical design requirement is whether it is necessary to obtain the positive-sequence voltage characteristics only (i.e. magnitude and phase angle), or both the positive-sequence and negative-sequence voltage characteristics. If the intention is to only obtain the positive-sequence characteristics, a variety of solutions exist to eliminate the ripple that is produced by the negative-sequence voltage. One common solution is to place a filter inside the positive-sequence loop or before the PLL. A review of three-phase PLLs with enhanced filtering capabilities is shown in [1], although some examples are: using a notch filter [15], using a moving average filter [16], or using a Delayed Signal Cancellation (DSC) approach [17]. These options are very efficient in terms of computational burden. However, if the negative-sequence characteristics are desired as well, these filtering methods might not be sufficient. In this case, different solutions have been proposed, for example: the DDSRF-PLL [2], the Dual Second Order Generalized Integrator PLL (DSOGI-PLL) [18], the three-phase Enhanced PLL (3ph-EPLL) [19], the use of Adaptive Notch Filters (ANFs) combined with a symmetrical components calculator [20], or the use of methods derived from optimization problems [21]. Some of these structures are analysed and compared in [22], where it is shown that the DDSRF-PLL has very good performance under unbalanced conditions. Since the DDSRF-PLL is very popular phase-tracking scheme in three-phase applications [1], it was selected as an example in this article for showcasing the LTI vs. LTP modelling techniques, although other methods could have been an interesting case study as well.

In particular, two DDSRF-PLL implementations (from now on, called methods for brevity) are shown, which are focused on tracking both the positive and negative-sequence phase-angle. In a broad context, the negative-sequence properties might be useful for monitoring purposes, fault analysis and

[1] It is worth to observe that, from a mathematical perspective, a single-phase voltage is equivalent to a three-phase voltage with considerable imbalance.

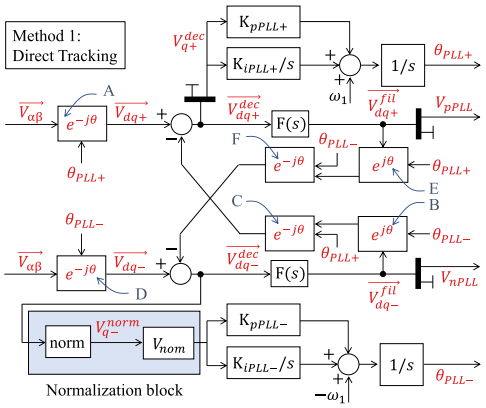

FIGURE 1. Method 1 (M1) for DDSRF-PLL implementation: Direct tracking of negative-sequence voltage phase-angle.

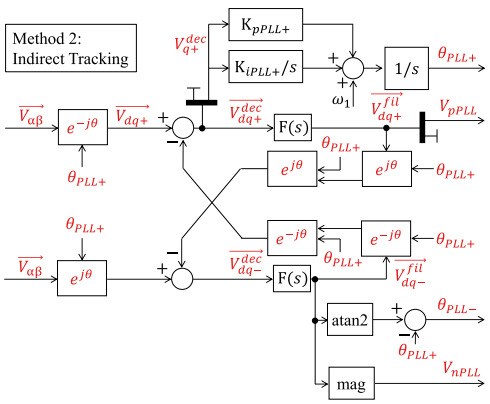

FIGURE 2. Method 2 (M2) for DDSRF-PLL implementation: Indirect tracking of negative-sequence voltage phase-angle.

classification, or other applications [21]. According to [20], extracting the characteristics of all the symmetrical components in the grid voltage is important for many applications, including power quality and protection. Another usage can be the calculation of synchrophasors [23]. In the energy conversion context, the negative-sequence characteristics can be useful, for example, for generating a negative-sequence SRF for controlling the negative-sequence current (a strategy common in wind energy generation [24], [25] and other applications [26], [27]).

The DDSRF-PLL methods are presented in Section II. The LTI and LTP models are derived in Section III – Section VI, and are validated in Section VII. An explanation of the LTI and LTP model differences is shown in Section VIII. The comparison of the LTI and LTP models for stability studies is shown in Section IX. Conclusions are in Section XII.

II. DESCRIPTION OF THE DDSRF-PLL METHODS

In this article, the phase-angle of the positive-sequence voltage is $\theta_{1+} = \omega_1 t + \phi_{vp}$, whereas for the negative-sequence is $\theta_{1-} = -\omega_1 t - \phi_{vn}$. The outputs of the PLL are θ_{PLL+} and θ_{PLL-}, which might not be exactly accurate, having some error as: $\theta_{PLL+} = \theta_{1+} + \Delta\theta_{1+}$ and $\theta_{PLL-} = \theta_{1-} + \Delta\theta_{1-}$.

A. METHOD 1: DIRECT TRACKING OF θ_{1-}

The schematic of method 1 (M1) is shown in Fig. 1. This method incorporates two separate SRF-PLLs, one for tracking the positive sequence and one for the negative sequence. The logic behind this design is to try to make the PLL as symmetrical as possible. This method is called direct tracking since it uses an SRF-PLL to directly track the negative sequence. The phase angle obtained by this SRF-PLL, θ_{PLL-}, is used within the decoupling network of the DDSRF-PLL, which means that, in steady state, the negative-sequence frame in the decoupling network rotates perfectly with $\theta_{1-} = -\omega_1 t - \phi_{vn}$. Thus, $\overrightarrow{V^{fil}_{dq-}}$ has, in steady state, V_n in the d channel and 0 in the q channel.

Usually, the nominal voltage (V_{nom}) is used for designing the parameters for the positive-sequence SRF-PLL (details in Appendix A). The input to the negative-sequence SRF-PLL, however, varies a lot, since V_n ranges from being very low in normal operating conditions to being very high during certain faults. For minimizing this effect, normalization can be performed as:

$$V^{norm}_{q-} = \frac{V^{dec}_{q-}}{\sqrt{(V^{dec}_{d-})^2 + (V^{dec}_{q-})^2}}. \tag{1}$$

Thus, if V^{norm}_{q-} is multiplied by V_{nom}, the same PLL constants can be used for the positive- and negative-sequence SRF-PLL.

B. METHOD 2: INDIRECT TRACKING OF θ_{1-}

The schematic of method 2 (M2) is shown in Fig. 2. This method uses only a positive-sequence SRF-PLL, and uses the phase-angle it creates, θ_{PLL+} in all the decoupling network transformations. This means that, in steady state, the negative-sequence frame in the decoupling network does not rotate with $\theta_{1-} = -\omega_1 t - \phi_{vn}$, but rather with $-\theta_{1+} = -\omega_1 t - \phi_{vp}$. When representing the negative-sequence voltage in such a frame, the space vector has the form $V_n e^{j(\phi_{vp}-\phi_{vn})}$. Note that, unless $\phi_{vp} = \phi_{vn}$, the signal that serves as input to the $atan2$ function does not have a q channel equal to 0. Therefore, the output of the $atan2$ function in Fig. 2 is, in steady state, equal to $\phi_{vp} - \phi_{vn}$. The θ_{PLL-}, then, can be obtained by subtracting θ_{PLL+} from the output of the $atan2$ function. This method is the DDSRF-PLL shown in [2] but with additional blocks to calculate θ_{PLL-} and V_n. This method is called indirect tracking since it only tracks directly θ_{1+}, while θ_{1-} is derived from the signals in the network.

III. LTP MODEL OF METHOD 1

In this article, the dq frame rotating with θ_{1+} is called ideal positive-sequence dq frame whereas the non-ideal one rotates at θ_{PLL+}. Similarly is defined for the negative sequence.

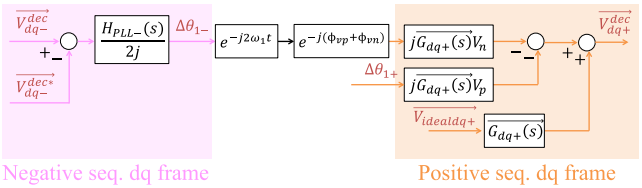

FIGURE 3. V_{dq+}^{dec} as a function of V_{dq-}^{dec}.

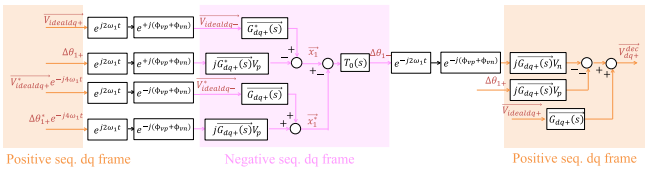

FIGURE 4. V_{dq+}^{dec} as a function of positive *dq* frame signals.

A. STEP 1: SOLVING THE DECOUPLING NETWORK

The first step is to analyse the transformations named A-F in Fig. 1. For the transformation A:

$$\begin{aligned}\overrightarrow{V_{\text{nonidealdq+}}} &= \overrightarrow{V_{\text{idealdq+}}} e^{-j\Delta\theta_{1+}} \approx \overrightarrow{V_{\text{idealdq+}}}(1 - j\Delta\theta_{1+}) \\ &= \overrightarrow{V_{\text{idealdq+}}} - jV_{\text{p}}\Delta\theta_{1+} - jV_{\text{n}}e^{-j(2\omega_1 t+\phi_{\text{vp}}+\phi_{\text{vn}})}\Delta\theta_{1+}. \quad (2)\end{aligned}$$

The input to transformation B is $\overrightarrow{V_{\text{dq-}}^{\text{fil}}}$, which in steady-state is approximately V_{n}. Thus, the output of this transformation in steady-state should be $V_{\text{n}}e^{-j(\omega_1 t+\phi_{\text{vn}})}$. Therefore:

$$\begin{aligned}\overrightarrow{V_{\text{B}_{\text{out}}}} &= \overrightarrow{V_{\text{dq-}}^{\text{fil}}} e^{j\theta_{1-}} e^{j\Delta\theta_{1-}} \approx \overrightarrow{V_{\text{dq-}}^{\text{fil}}} e^{j\theta_{1-}} \\ &\quad + jV_{\text{n}}e^{-j(\omega_1 t+\phi_{\text{vn}})}\Delta\theta_{1-}. \quad (3)\end{aligned}$$

The transformations C, D, E and F can be found similarly. Taking into account all transformations, it can be found:

$$\begin{aligned}\overrightarrow{V_{\text{dq+}}^{\text{dec}}} &= \overrightarrow{G_{\text{dq+}}(s)}(\overrightarrow{V_{\text{idealdq+}}} - jV_{\text{p}}\Delta\theta_{1+} \\ &\quad - jV_{\text{n}}e^{-j(\phi_{\text{vp}}+\phi_{\text{vn}})}\Delta\theta_{1-}e^{-j2\omega_1 t}) \quad (4)\\ \overrightarrow{V_{\text{dq-}}^{\text{dec}}} &= \overrightarrow{G_{\text{dq+}}^{*}(s)}(\overrightarrow{V_{\text{idealdq-}}} - jV_{\text{n}}\Delta\theta_{1-} \\ &\quad - jV_{\text{p}}e^{+j(\phi_{\text{vp}}+\phi_{\text{vn}})}\Delta\theta_{1+}e^{+j2\omega_1 t}) \quad (5)\end{aligned}$$

where

$$\overrightarrow{G_{\text{dq+}}(s)} = \frac{1 - F(s + j2\omega_1)}{1 - F(s)F(s + j2\omega_1)}. \quad (6)$$

Additionally, if it is defined $H_{\text{PLL+}}(s) = \left[K_{\text{pPLL+}} + \frac{K_{\text{iPLL+}}}{s}\right]\frac{1}{s}$ (and similarly for the negative sequence) from the schematic in Fig. 1, it is straightforward to find:[2]

$$\Delta\theta_{1+} = V_{\text{q+}}^{\text{dec}} H_{\text{PLL+}}(s) = \frac{1}{2j}(\overrightarrow{V_{\text{dq+}}^{\text{dec}}} - \overrightarrow{V_{\text{dq+}}^{\text{dec}*}})H_{\text{PLL+}}(s) \quad (7)$$

$$\Delta\theta_{1-} = V_{\text{q-}}^{\text{dec}} H_{\text{PLL-}}(s) = \frac{1}{2j}(\overrightarrow{V_{\text{dq-}}^{\text{dec}}} - \overrightarrow{V_{\text{dq-}}^{\text{dec}*}})H_{\text{PLL-}}(s). \quad (8)$$

Combining (7) and (8) with (4) and (5) is not simple since both (4) and (5) depend on both $\Delta\theta_{1+}$ and $\Delta\theta_{1-}$.

B. STEP 2: EXPRESSING V_{DQ+}^{DEC} AS A FUNCTION OF $\Delta\theta_{1+}$ ONLY

Substituting (8) into (4) leads to the schematic in Fig. 3. An auxiliary term $\overrightarrow{x_1}$ can be defined such that:

$$\overrightarrow{x_1} = \overrightarrow{G_{\text{dq+}}^{*}(s)}(\overrightarrow{V_{\text{idealdq-}}} - jV_{\text{p}}e^{+j(\phi_{\text{vp}}+\phi_{\text{vn}})}\Delta\theta_{1+}e^{+j2\omega_1 t}) \quad (9)$$

This means that:

$$\overrightarrow{V_{\text{dq-}}^{\text{dec}}} = \overrightarrow{x_1} - \overrightarrow{G_{\text{dq+}}^{*}(s)}jV_{\text{n}}\Delta\theta_{1-}. \quad (10)$$

Using (10) and its conjugate in (8) and operating leads to:

$$\Delta\theta_{1-} = (\overrightarrow{x_1} - \overrightarrow{x_1^{*}})\underbrace{\frac{H_{\text{PLL-}}(s)}{2j(1 + V_{\text{n}}H_{\text{PLL-}}(s)G_{\text{re}}(s))}}_{T_0(s)}. \quad (11)$$

Using (9) and (11), Fig. 3 can be transformed intoFig. 4.[3] The transfer functions that appear in Fig. 4 in the negative *dq* frame can be easily taken into the positive *dq* frame with a frequency shift [28]. This leads to the following equation:

$$\begin{aligned}\overrightarrow{V_{\text{dq+}}^{\text{dec}}} &= \overrightarrow{V_{\text{idealdq+}}}\overrightarrow{T_1} + \Delta\theta_{1+}\overrightarrow{T_2} \\ &\quad + \overrightarrow{V_{\text{idealdq+}}^{*}}e^{-j4\omega_1 t}\overrightarrow{T_3} + \Delta\theta_{1+}e^{-j4\omega_1 t}\overrightarrow{T_4} \quad (12)\end{aligned}$$

where $\overrightarrow{T_1}$–$\overrightarrow{T_4}$ are defined in Appendix B.

C. STEP 3: FINAL EXPRESSION FOR $\Delta\theta_{1+}$

The expression (12) can be plugged into (7), and after operating, the following expression is obtained:

$$\begin{aligned}\Delta\theta_{1+} = \overrightarrow{T_5}[&\overrightarrow{V_{\text{idealdq+}}}\overrightarrow{T_1} - \overrightarrow{V_{\text{idealdq+}}^{*}}\overrightarrow{T_1^{*}} + \overrightarrow{V_{\text{idealdq+}}^{*}}e^{-j4\omega_1 t}\overrightarrow{T_3} \\ &- \overrightarrow{V_{\text{idealdq+}}}e^{+j4\omega_1 t}\overrightarrow{T_3^{*}} + \Delta\theta_{1+}e^{-j4\omega_1 t}\overrightarrow{T_4} \\ &- \Delta\theta_{1+}e^{+j4\omega_1 t}\overrightarrow{T_4^{*}}]. \quad (13)\end{aligned}$$

where $\overrightarrow{T_5}$ is defined in Appendix B. The expression (13) clearly reveals the LTP dynamics of the PLL. If the voltage (in the positive *dq* frame) has a component at a frequency ω, then the $\Delta\theta_{1+}$ will have the components[4] $\pm\omega$, which in turn will create in a feedback loop through $\overrightarrow{T_4}$ and $\overrightarrow{T_4^{*}}$ the frequencies $\pm\omega \pm 4\omega_1$. Note that this is a theoretically infinite procedure, in which $\pm\omega \pm 4\omega_1$ will create also a new frequencies at $\pm\omega \pm 8\omega_1$; etc. In Fig. 5 the main frequency paths (i.e. at the frequencies $\pm\omega$, $\pm\omega \pm 4\omega_1$) are shown.

If other frequency components are neglected (this is further discussed in Section IX), then it is possible to solve the equations for each frequency path shown in Fig. 5. The direct path

[2]The normalization block is ignored for now but it is included later.

[3]In Fig. 4, $\Delta\theta_{1+}^{*}$ appears although $\Delta\theta_{1+}^{*}$=$\Delta\theta_{1+}$ since $\Delta\theta_{1+}$ is not a vector.

[4]As an example, if $\Delta\theta_{1+}$ has the component $A\cos(\omega t)$ this can only be represented in vector form as $\frac{A}{2}e^{j\omega t} + \frac{A}{2}e^{-j\omega t}$.

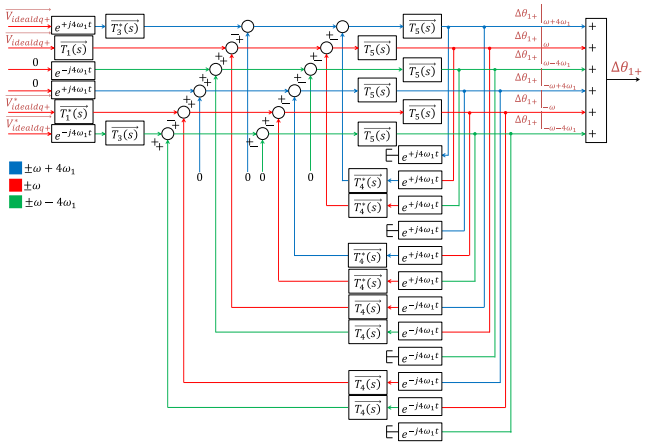

FIGURE 5. Schematic of equation (13), which clearly reveals the LTP dynamics of the PLL.

(at frequency ω) leads to:

$$\Delta\theta_{1+}|_{\omega} = \underbrace{\frac{c_1 + d_1}{1 + a_1 + b_1}}_{\overrightarrow{TF_{\text{PLL1+}}(s)}} \overrightarrow{V_{\text{idealdq+}}} \tag{14}$$

with:

$$\begin{aligned} a_1 &= \overrightarrow{T_4^*(s + j4\omega_1)}\overrightarrow{T_5(s + j4\omega_1)}\overrightarrow{T_4}\,\overrightarrow{T_5} \\ b_1 &= \overrightarrow{T_4(s - j4\omega_1)}\overrightarrow{T_5(s - j4\omega_1)}\overrightarrow{T_4^*}\,\overrightarrow{T_5} \\ c_1 &= \overrightarrow{T_1}\,\overrightarrow{T_5} \\ d_1 &= -\overrightarrow{T_3^*(s + j4\omega_1)}\overrightarrow{T_5(s + j4\omega_1)}\overrightarrow{T_4}\,\overrightarrow{T_5}. \end{aligned} \tag{15}$$

Solving the conjugate frequencies leads to:

$$\Delta\theta_{1+}|_{-\omega} = \underbrace{\frac{c_2 + d_2}{1 + a_2 + b_2}}_{\overrightarrow{TF_{\text{PLL2+}}(s)}} \overrightarrow{V^*_{\text{idealdq+}}} \tag{16}$$

with:

$$\begin{aligned} a_2 &= a_1\,;\; b_2 = b_1\,;\; c_2 = -\overrightarrow{T_1^*}\,\overrightarrow{T_5} \\ d_2 &= -\overrightarrow{T_3(s - j4\omega_1)}\overrightarrow{T_5(s - j4\omega_1)}\overrightarrow{T_4^*}\,\overrightarrow{T_5}. \end{aligned} \tag{17}$$

The other frequencies in $\Delta\theta_{1+}$ can be solved now, leading to the final model of the DDSRF-PLL for the positive-sequence phase-angle as shown in (18).

$$\begin{aligned} \Delta\theta_{1+} \approx\; & \overrightarrow{V_{\text{idealdq+}}}\overrightarrow{TF_{\text{PLL1+}}} + \overrightarrow{V^*_{\text{idealdq+}}}\overrightarrow{TF_{\text{PLL2+}}} \\ & + \overrightarrow{V_{\text{idealdq+}}e^{j4\omega_1 t}}\overrightarrow{TF_{\text{PLL3+}}} + (\overrightarrow{V_{\text{idealdq+}}e^{j4\omega_1 t}})^*\overrightarrow{TF_{\text{PLL4+}}} \\ & + \overrightarrow{V_{\text{idealdq+}}e^{-j4\omega_1 t}}\overrightarrow{TF_{\text{PLL5+}}} + (\overrightarrow{V_{\text{idealdq+}}e^{-j4\omega_1 t}})^*\overrightarrow{TF_{\text{PLL6+}}} \end{aligned} \tag{18}$$

(18) uses an approximate sign, since in reality there are an infinite number of PLL couplings. In here, only the first round of couplings is shown. The question as to how many couplings need to be included is answered in Section IX-F.

D. STEP 4: NEGATIVE-SEQUENCE PHASE-ANGLE MODEL

The final model for the negative-sequence phase-angle can be similarly derived and it is shown in (19).

$$\begin{aligned} \Delta\theta_{1-} \approx\; & \overrightarrow{V_{\text{idealdq-}}}\overrightarrow{TF_{\text{PLL1-}}} + \overrightarrow{V^*_{\text{idealdq-}}}\overrightarrow{TF_{\text{PLL2-}}} \\ & + \overrightarrow{V_{\text{idealdq-}}e^{-j4\omega_1 t}}\overrightarrow{TF_{\text{PLL3-}}} + (\overrightarrow{V_{\text{idealdq-}}e^{-j4\omega_1 t}})^*\overrightarrow{TF_{\text{PLL4-}}} \\ & + \overrightarrow{V_{\text{idealdq-}}e^{j4\omega_1 t}}\overrightarrow{TF_{\text{PLL5-}}} + (\overrightarrow{V_{\text{idealdq-}}e^{j4\omega_1 t}})^*\overrightarrow{TF_{\text{PLL6-}}} \end{aligned} \tag{19}$$

It can be shown that $\overrightarrow{TF_{\text{PLL2+}}(s)} = \overrightarrow{TF^*_{\text{PLL1+}}(s)}$, $\overrightarrow{TF_{\text{PLL4+}}(s)} = \overrightarrow{TF^*_{\text{PLL3+}}(s)}$ and $\overrightarrow{TF_{\text{PLL6+}}(s)} = \overrightarrow{TF^*_{\text{PLL5+}}(s)}$. The same applies for the complex transfer functions in (19).

E. STEP 5: INCLUDING NORMALIZATION

For including the normalization block shown in Fig. 1, it is necessary to linearise (1) through a Taylor series expansion (around the steady-state operating point $(V_{\text{n}}, 0)$). The result is:

$$V^{\text{norm}}_{\text{q-}} \approx \frac{V^{\text{dec}}_{\text{q-}}}{V_{\text{n}}}. \tag{20}$$

Thus, for including the normalization block, the only step is to substitute $H_{\text{PLL-}}(s)$ by $\frac{V_{\text{nom}}H_{\text{PLL-}}(s)}{V_{\text{n}}}$ in all equations.

IV. LTI MODEL OF METHOD 1

For developing the LTI model, the time-varying coefficients are ignored. In method 1, this means that (4) and (5) become:

$$\overrightarrow{V^{\text{dec}}_{\text{dq+}}} = \overrightarrow{G_{\text{dq+}}(s)}(\overrightarrow{V_{\text{idealdq+}}} - jV_{\text{p}}\Delta\theta_{1+}) \tag{21}$$

$$\overrightarrow{V^{\text{dec}}_{\text{dq-}}} = \overrightarrow{G^*_{\text{dq+}}(s)}(\overrightarrow{V_{\text{idealdq-}}} - jV_{\text{n}}\Delta\theta_{1-}) \tag{22}$$

Combining these expressions with (7) and (8) is straightforward, and leads to the following model:

$$\begin{aligned} \Delta\theta_{1+} &= \overrightarrow{V_{\text{idealdq+}}}\overrightarrow{TF_{\text{PLL1+LTI}}} + \overrightarrow{V^*_{\text{idealdq+}}}\overrightarrow{TF_{\text{PLL2+LTI}}} \\ \Delta\theta_{1-} &= \overrightarrow{V_{\text{idealdq-}}}\overrightarrow{TF_{\text{PLL1-LTI}}} + \overrightarrow{V^*_{\text{idealdq-}}}\overrightarrow{TF_{\text{PLL2-LTI}}} \end{aligned} \tag{23}$$

$$\begin{aligned} \overrightarrow{TF_{\text{PLL1+LTI}}} &= \frac{H_{\text{PLL+}}(s)\overrightarrow{G_{\text{dq+}}(s)}}{2j(1 + V_{\text{p}}H_{\text{PLL+}}(s)G_{\text{re}}(s))} \\ \overrightarrow{TF_{\text{PLL1-LTI}}} &= \frac{H_{\text{PLL-}}(s)\overrightarrow{G^*_{\text{dq+}}(s)}}{2j(1 + V_{\text{n}}H_{\text{PLL-}}(s)G_{\text{re}}(s))} \end{aligned} \tag{24}$$

where $\overrightarrow{TF_{\text{PLL2+LTI}}} = \overrightarrow{TF^*_{\text{PLL1+LTI}}}$, $\overrightarrow{TF_{\text{PLL2-LTI}}} = \overrightarrow{TF^*_{\text{PLL1-LTI}}}$. For including the normalization block, the same steps as explained for the LTP model (Section III-E) should be taken.

V. LTP MODEL OF METHOD 2

A. STEP 1: SOLVING THE DECOUPLING NETWORK

In a similar process as it is done with the method 1, the following equations can be obtained for the method 2:

$$\overrightarrow{V^{\text{dec}}_{\text{dq+}}} = \overrightarrow{G_{\text{dq+}}(s)}(\overrightarrow{V_{\text{idealdq+}}} - jV_{\text{p}}\Delta\theta_{1+} + jV_{\text{n}}e^{-j(\phi_{\text{vp}}+\phi_{\text{vn}})}\Delta\theta_{1+}e^{-j2\omega_1 t}) \tag{25}$$

$$\overrightarrow{V^{\text{dec}}_{\text{dq-}}} = \overrightarrow{G^{*}_{\text{dq+}}(s)}e^{+j(\phi_{\text{vp}}-\phi_{\text{vn}})}(\overrightarrow{V_{\text{idealdq-}}} + jV_{\text{n}}\Delta\theta_{1+} - jV_{\text{p}}e^{+j(\phi_{\text{vp}}+\phi_{\text{vn}})}\Delta\theta_{1+}e^{+j2\omega_1 t}) \tag{26}$$

In this case, $\Delta\theta_{1-}$ does not appear in (25) nor in (26), since the decoupling network only uses $\theta_{\text{PLL+}}$. In (26) there is a new term, $e^{+j(\phi_{\text{vp}}-\phi_{\text{vn}})}$, that does not appear in the equations of M1. This term is here because, in the M2, the $\overrightarrow{V^{\text{dec}}_{\text{dq-}}}$ is a signal that ideally rotates with $-\theta_{1+} = -\omega_1 t - \phi_{\text{vp}}$, instead of rotating with $\theta_{1-} = -\omega_1 t - \phi_{\text{vn}}$ as in method 1.

B. STEP 2: FINAL EXPRESSION FOR $\Delta\theta_{1+}$

The expression (25) can be used in (7). Operating leads to:

$$\Delta\theta_{1+} = \overrightarrow{T_6}[\overrightarrow{V_{\text{idealdq+}}}\overrightarrow{G_{\text{dq+}}(s)} - \overrightarrow{V^{*}_{\text{idealdq+}}}\overrightarrow{G^{*}_{\text{dq+}}(s)} + \Delta\theta_{1+}e^{+j2\omega_1 t}\overrightarrow{T_7} - \Delta\theta_{1+}e^{-j2\omega_1 t}\overrightarrow{T^{*}_7}]. \tag{27}$$

where $\overrightarrow{T_6}$ and $\overrightarrow{T_7}$ are defined in Appendix C. Similarly as with method 1, the expression (27) reveals LTP dynamics, although this time they are dependent on $\pm 2\omega_1$ instead of $\pm 4\omega_1$. Performing similar operations and schematics as with method 1, the following LTP model can be obtained:

$$\Delta\theta_{1+} \approx \overrightarrow{V_{\text{idealdq+}}}\overrightarrow{TF_{\text{PLL1+}}} + \overrightarrow{V^{*}_{\text{idealdq+}}}\overrightarrow{TF_{\text{PLL2+}}} + \overrightarrow{V_{\text{idealdq+}}}e^{j2\omega_1 t}\overrightarrow{TF_{\text{PLL3+}}} + (\overrightarrow{V_{\text{idealdq+}}}e^{j2\omega_1 t})^{*}\overrightarrow{TF_{\text{PLL4+}}} + \overrightarrow{V_{\text{idealdq+}}}e^{-j2\omega_1 t}\overrightarrow{TF_{\text{PLL5+}}} + (\overrightarrow{V_{\text{idealdq+}}}e^{-j2\omega_1 t})^{*}\overrightarrow{TF_{\text{PLL6+}}} \tag{28}$$

C. STEP 3: NEGATIVE-SEQUENCE PHASE-ANGLE MODEL

Here, it is necessary to linearise $atan\left(\frac{V^{\text{fil}}_{\text{q-}}}{V^{\text{fil}}_{\text{d-}}}\right)$ around the point $(\Im\{V_{\text{n}}e^{+j(\phi_{\text{vp}}-\phi_{\text{vn}})}\}, \Re\{V_{\text{n}}e^{+j(\phi_{\text{vp}}-\phi_{\text{vn}})}\})$. This results in:

$$atan\left(\frac{V^{\text{fil}}_{\text{q-}}}{V^{\text{fil}}_{\text{d-}}}\right) \approx \phi_{\text{vp}} - \phi_{\text{vn}} + \frac{(e^{+j(\phi_{\text{vp}}-\phi_{\text{vn}})} + e^{-j(\phi_{\text{vp}}-\phi_{\text{vn}})})}{2V_{\text{n}}}V^{\text{fil}}_{\text{q-}} - \frac{(e^{+j(\phi_{\text{vp}}-\phi_{\text{vn}})} - e^{-j(\phi_{\text{vp}}-\phi_{\text{vn}})})}{j2V_{\text{n}}}V^{\text{fil}}_{\text{d-}}. \tag{29}$$

Since $\theta_{\text{PLL-}} = -\theta_{\text{PLL+}} + atan\left(\frac{V^{\text{fil}}_{\text{q-}}}{V^{\text{fil}}_{\text{d-}}}\right)$, and also $\theta_{\text{PLL+}} = \omega_1 t + \phi_{\text{vp}} + \Delta\theta_{1+}$ and $\theta_{\text{PLL-}} = -\omega_1 t - \phi_{\text{vn}} + \Delta\theta_{1-}$, then:

$$\Delta\theta_{1-} = -\Delta\theta_{1+} + \frac{(e^{+j(\phi_{\text{vp}}-\phi_{\text{vn}})} + e^{-j(\phi_{\text{vp}}-\phi_{\text{vn}})})}{2V_{\text{n}}}V^{\text{fil}}_{\text{q-}} - \frac{(e^{+j(\phi_{\text{vp}}-\phi_{\text{vn}})} - e^{-j(\phi_{\text{vp}}-\phi_{\text{vn}})})}{j2V_{\text{n}}}V^{\text{fil}}_{\text{d-}}. \tag{30}$$

Knowing that $\overrightarrow{V^{\text{fil}}_{\text{dq-}}} = F(s)\overrightarrow{V^{\text{dec}}_{\text{dq-}}}$, the terms $V^{\text{fil}}_{\text{d-}}$ and $V^{\text{fil}}_{\text{q-}}$ can be derived from (26), while $\Delta\theta_{1+}$ is shown in (28). The final LTP model for $\Delta\theta_{1-}$ for method 2 is:

$$\Delta\theta_{1-} \approx \overrightarrow{V_{\text{idealdq-}}}\overrightarrow{TF_{\text{PLL1-}}} + \overrightarrow{V^{*}_{\text{idealdq-}}}\overrightarrow{TF_{\text{PLL2-}}} + \overrightarrow{V_{\text{idealdq-}}}e^{-j2\omega_1 t}\overrightarrow{TF_{\text{PLL3-}}} + (\overrightarrow{V_{\text{idealdq-}}}e^{-j2\omega_1 t})^{*}\overrightarrow{TF_{\text{PLL4-}}} + \overrightarrow{V_{\text{idealdq-}}}e^{+j2\omega_1 t}\overrightarrow{TF_{\text{PLL5-}}} + (\overrightarrow{V_{\text{idealdq-}}}e^{+j2\omega_1 t})^{*}\overrightarrow{TF_{\text{PLL6-}}} \tag{31}$$

VI. LTI MODEL OF METHOD 2

For developing the LTI model, the time-varying coefficients are ignored. Thus, (25) and (26) become:

$$\overrightarrow{V^{\text{dec}}_{\text{dq+}}} = \overrightarrow{G_{\text{dq+}}(s)}(\overrightarrow{V_{\text{idealdq+}}} - jV_{\text{p}}\Delta\theta_{1+}) \tag{32}$$

$$\overrightarrow{V^{\text{dec}}_{\text{dq-}}} = \overrightarrow{G^{*}_{\text{dq+}}(s)}e^{+j(\phi_{\text{vp}}-\phi_{\text{vn}})}(\overrightarrow{V_{\text{idealdq-}}} + jV_{\text{n}}\Delta\theta_{1+}) \tag{33}$$

Since (32) is the same as (21), the LTI model of $\Delta\theta_{1+}$ is the same in method 2 as in method 1. For $\Delta\theta_{1-}$, knowing that $\overrightarrow{V^{\text{fil}}_{\text{dq-}}} = F(s)\overrightarrow{V^{\text{dec}}_{\text{dq-}}}$, it is necessary to use (33) in (30) and, ignoring oscillating terms, the LTI model results in:

$$\Delta\theta_{1-} = \overrightarrow{V_{\text{idealdq-}}}\overrightarrow{TF_{\text{PLL1-LTI}}} + \overrightarrow{V^{*}_{\text{idealdq-}}}\overrightarrow{TF_{\text{PLL2-LTI}}} \tag{34}$$

where $\overrightarrow{TF_{\text{PLL2-LTI}}} = \overrightarrow{TF^{*}_{\text{PLL1-LTI}}}$ and

$$\overrightarrow{TF_{\text{PLL1-LTI}}} = \frac{1}{2jV_{\text{n}}}(F(s)\overrightarrow{G^{*}_{\text{dq+}}(s)}). \tag{35}$$

VII. VALIDATION OF LTI AND LTP MODELS

A. TIME DOMAIN VALIDATION

The models are validated with time-domain simulations. The PLL parameters in Appendix A are used, and also $K = 1/\sqrt{2}$. Three tests are performed:

- *Test 1:* From a steady-state operating point with $V_{\text{n}} = 5\%$, V_{n} is increased 10% of its value (small-signal perturbation).
- *Test 2:* From a steady-state operating point with $V_{\text{n}} = 60\%$, V_{n} is increased 10% of its value (small-signal perturbation).
- *Test 3:* From a steady-state operating point with $V_{\text{n}} = 5\%$, V_{n} is increased until $V_{\text{n}} = 60\%$ (large-signal perturbation).

The results for the DDSRF-PLL method 1 are shown in Fig. 6. It can be seen that, for small-signal perturbations (Test 1 and Test 2), the LTI model fails to predict the oscillations that appear in the phase angles. The LTI model predicts a much cleaner and stable response than what the simulations show. The LTP model, however, perfectly predicts the trend for small-signal perturbations. In the Test 3, where there is a large-signal perturbation, the LTI model again is inaccurate. For the LTP model, the positive-sequence phase-angle transient is perfectly predicted, but not the negative-sequence one.

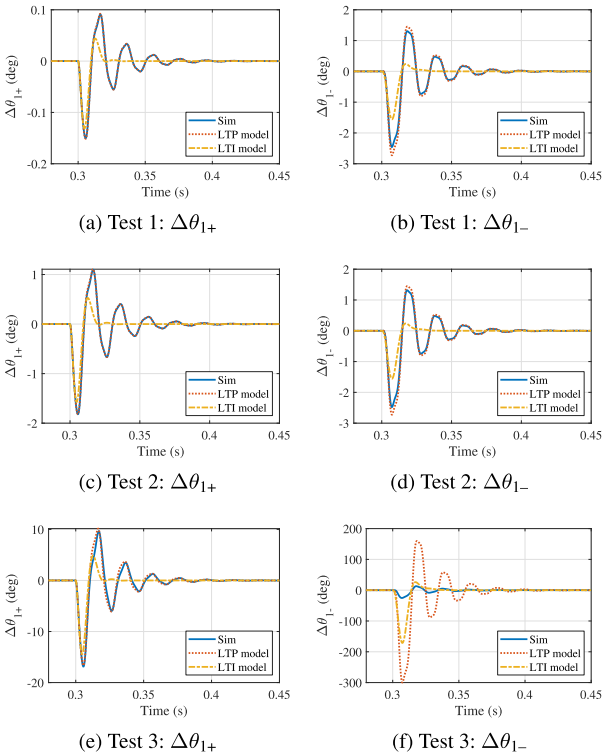

(a) Test 1: $\Delta\theta_{1+}$ (b) Test 1: $\Delta\theta_{1-}$

(c) Test 2: $\Delta\theta_{1+}$ (d) Test 2: $\Delta\theta_{1-}$

(e) Test 3: $\Delta\theta_{1+}$ (f) Test 3: $\Delta\theta_{1-}$

FIGURE 6. Validation of LTI and LTP models for method 1 in the time domain.

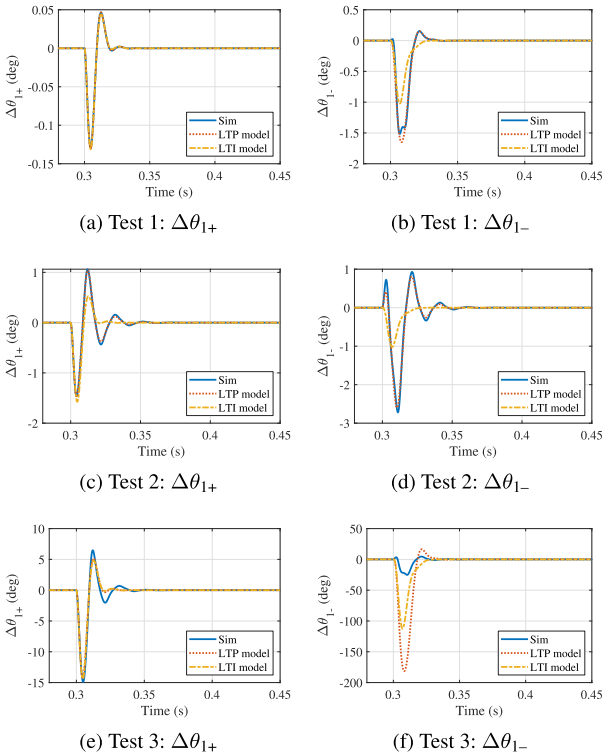

(a) Test 1: $\Delta\theta_{1+}$ (b) Test 1: $\Delta\theta_{1-}$

(c) Test 2: $\Delta\theta_{1+}$ (d) Test 2: $\Delta\theta_{1-}$

(e) Test 3: $\Delta\theta_{1+}$ (f) Test 3: $\Delta\theta_{1-}$

FIGURE 7. Validation of LTI and LTP models for method 2 in the time domain.

This test shows that, even if periodic, the LTP model is still small-signal.

Fig. 7 analyses the DDSRF-PLL method 2. Test 1 shows that the LTI model can predict the transient of a small-signal perturbation if V_n is low (at least for $\Delta\theta_{1+}$). However, if V_n is increased (Test 2), the LTI model is no longer small-signal accurate. Just like in method 1, the LTI model underestimates the oscillations. In contrast, the LTP model follows the transient after a small-signal perturbation no matter the V_n level. In Test 3, both models are inaccurate since both models are linearised.

B. FREQUENCY DOMAIN VALIDATION

Different frequency sweeps were performed for different V_n levels. The results are shown in Fig. 8 (method 1). Certain transfer functions are not shown since they are conjugates of the transfer functions displayed. Fig. 8 shows that the LTP model is perfectly accurate for different levels of voltage imbalance, while the LTI model does not have a perfect overlap with the frequency scan. The model for method 2 is also validated (Fig. 9). Both figures use the parameters in Appendix A, and also $K = 1/\sqrt{2}$.

VIII. DIFFERENCES BETWEEN THE LTI AND LTP MODELS

In (18) and (23), it appears as if the only difference between the LTI and LTP model is that the LTP model predicts the couplings, while the LTI model does not. However, this is not the main difference. For illustration purposes, the time-domain Test 1 results for method 1 are analysed in detail. Fig. 10 shows the decomposition of the time-domain response of the LTP model, according to the contribution to the total response by each of its transfer functions. The black dotted line in Fig. 10 corresponds to the LTP line shown in Fig. 6 a). As it can be seen, the coupling transfer functions contribute to the response; however, the biggest contribution comes from $\overrightarrow{TF_{\text{PLL1+}}}$ and $\overrightarrow{TF_{\text{PLL2+}}}$, and in fact, the total response of the LTP model (summing the responses of all transfer functions) is relatively similar to the response that the model would give if only $\overrightarrow{TF_{\text{PLL1+}}}$ and $\overrightarrow{TF_{\text{PLL2+}}}$ would be considered. Further, it is important to notice that the response given by $\overrightarrow{TF_{\text{PLL1+}}}$ and $\overrightarrow{TF_{\text{PLL2+}}}$ is not at all similar to such given by $\overrightarrow{TF_{\text{PLL1+LTI}}}$ and $\overrightarrow{TF_{\text{PLL2+LTI}}}$, which is shown in Fig. 6 a) (under the label LTI model). This is due to the fact that $\overrightarrow{TF_{\text{PLL1+}}}$ and $\overrightarrow{TF_{\text{PLL2+}}}$ are very different transfer functions than $\overrightarrow{TF_{\text{PLL1+LTI}}}$ and $\overrightarrow{TF_{\text{PLL2+LTI}}}$. This can be seen in the fact that the expression for $\overrightarrow{TF_{\text{PLL1+}}}$ (shown in (14)) is very different from the expression for $\overrightarrow{TF_{\text{PLL1+LTI}}}$ (shown in (24)). The transfer functions are different, and therefore they have different poles and stability properties. Therefore, the main difference between the LTI and LTP models is not that the LTP model predicts the couplings but that, through $\overrightarrow{TF_{\text{PLL1+}}}$ and $\overrightarrow{TF_{\text{PLL2+}}}$, it is able to predict important oscillatory behaviour that appears in the PLL in the presence of imbalance.

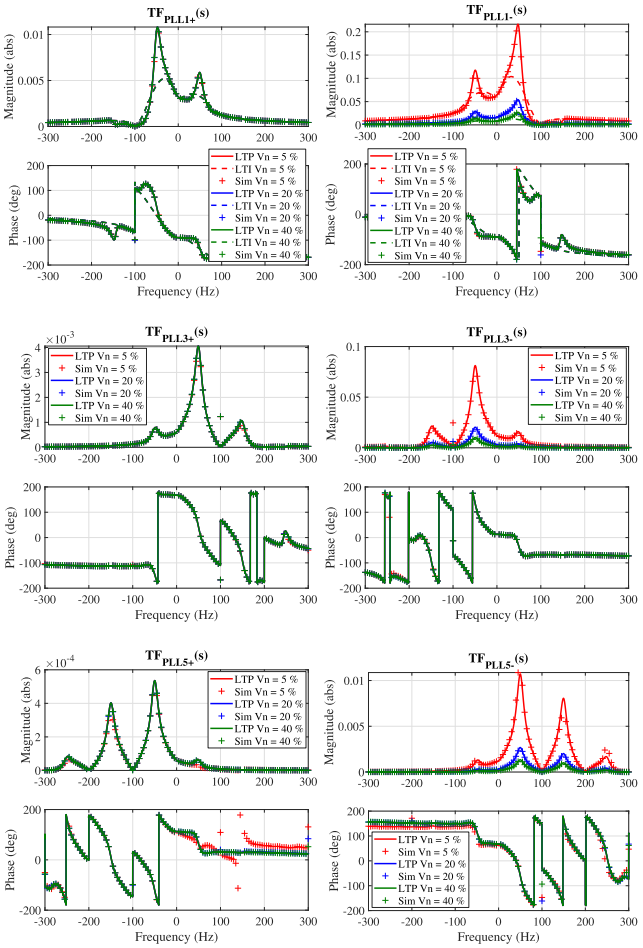

FIGURE 8. Validation of LTI and LTP models for method 1 in the frequency domain.

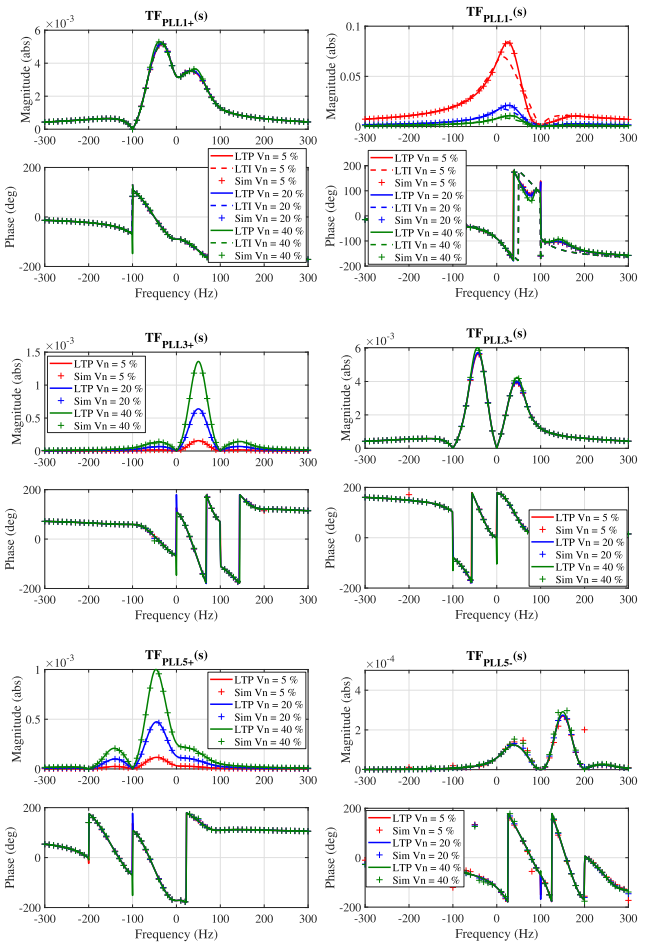

FIGURE 9. Validation of LTI and LTP models for method 2 in the frequency domain.

IX. STABILITY ANALYSIS

A. STABILITY ANALYSIS WITH THE LTI MODEL

The LTI and LTP models have two subsystems: one for the positive sequence and one for the negative sequence. In method 1, the LTI model for the positive sequence can be written as (36) and for the negative sequence as (37).

$$\begin{bmatrix} \Delta\theta_{1+} \\ \Delta\theta^*_{1+} \end{bmatrix} = [M_{\text{LTI1+}}]_{2x2} \begin{bmatrix} \overrightarrow{V_{\text{idealdq+}}} \\ \overrightarrow{V^*_{\text{idealdq+}}} \end{bmatrix} \tag{36}$$

$$\begin{bmatrix} \Delta\theta_{1-} \\ \Delta\theta^*_{1-} \end{bmatrix} = [M_{\text{LTI1-}}]_{2x2} \begin{bmatrix} \overrightarrow{V_{\text{idealdq-}}} \\ \overrightarrow{V^*_{\text{idealdq-}}} \end{bmatrix} \tag{37}$$

$M_{\text{LTI1+}}$ is a 2x2 complex transfer function matrix derived from (23). $M_{\text{LTI1+}}$ is shown in (38). $M_{\text{LTI1-}}$ can be found analogously.

$$M_{\text{LTI1+}} = \begin{bmatrix} \overrightarrow{TF_{\text{PLL1+LTI}}(s)} & \overrightarrow{TF_{\text{PLL2+LTI}}(s)} \\ \overrightarrow{TF^*_{\text{PLL2+LTI}}(s)} & \overrightarrow{TF^*_{\text{PLL1+LTI}}(s)} \end{bmatrix} \tag{38}$$

According to multivariable stability theory, in order to evaluate the stability with a MIMO LTI model, the MIMO poles of $M_{\text{LTI1+}}$ and $M_{\text{LTI1-}}$ need to be found, and all should lay in the Left Half Plane (LHP) [29].[5]

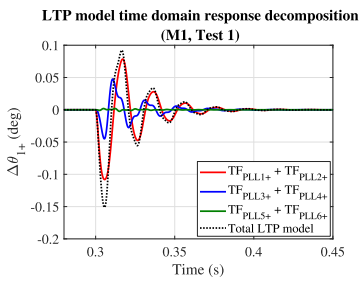

FIGURE 10. Decomposition of LTP model response (M1, Test 1).

[5]In a MIMO LTI system, there are two main ways of calculating the poles. The first one is to calculate the Smith-McMillan form of the transfer function matrix, a canonical form in which the poles are directly accessible [29]. Another option is to plot together all the poles of each individual transfer function in the matrix. This option gives the correct placement of the poles of the MIMO system, although the multiplicities of the poles are unknown. The second option is used in this article since the computations are faster, and since the multiplicities of the poles are not relevant (i.e. it is not important to know the number of poles in the RHP, but only whether there is any pole there).

B. STABILITY ANALYSIS WITH THE LTP MODEL

In the LTP model, the positive and negative sequence sub-systems are shown in (39) and (40), respectively. $M_{\text{LTP1+}}$ is a complex transfer function matrix derived from (18). The resulting matrix is (41) shown at the bottom of this page. $M_{\text{LTP1-}}$ can be found analogously.

$$\begin{bmatrix} \Delta\theta_{1+} \\ \Delta\theta^*_{1+} \\ \Delta\theta_{1+}e^{+j4\omega_1 t} \\ \Delta\theta^*_{1+}e^{-j4\omega_1 t} \\ \Delta\theta_{1+}e^{-j4\omega_1 t} \\ \Delta\theta^*_{1+}e^{+j4\omega_1 t} \end{bmatrix} = [M_{\text{LTP1+}}]_{6x6} \begin{bmatrix} \overrightarrow{V_{\text{idealdq+}}} \\ \overrightarrow{V^*_{\text{idealdq+}}} \\ \overrightarrow{V_{\text{idealdq+}}}e^{+j4\omega_1 t} \\ \overrightarrow{V^*_{\text{idealdq+}}}e^{-j4\omega_1 t} \\ \overrightarrow{V_{\text{idealdq+}}}e^{-j4\omega_1 t} \\ \overrightarrow{V^*_{\text{idealdq+}}}e^{+j4\omega_1 t} \end{bmatrix} \tag{39}$$

$$\begin{bmatrix} \Delta\theta_{1-} \\ \Delta\theta^*_{1-} \\ \Delta\theta_{1-}e^{-j4\omega_1 t} \\ \Delta\theta^*_{1-}e^{+j4\omega_1 t} \\ \Delta\theta_{1-}e^{+j4\omega_1 t} \\ \Delta\theta^*_{1-}e^{-j4\omega_1 t} \end{bmatrix} = [M_{\text{LTP1-}}]_{6x6} \begin{bmatrix} \overrightarrow{V_{\text{idealdq-}}} \\ \overrightarrow{V^*_{\text{idealdq-}}} \\ \overrightarrow{V_{\text{idealdq-}}}e^{-j4\omega_1 t} \\ \overrightarrow{V^*_{\text{idealdq-}}}e^{+j4\omega_1 t} \\ \overrightarrow{V_{\text{idealdq-}}}e^{+j4\omega_1 t} \\ \overrightarrow{V^*_{\text{idealdq-}}}e^{-j4\omega_1 t} \end{bmatrix} \tag{40}$$

The $M_{\text{LTP1+}}$ and $M_{\text{LTP1-}}$ shown in (39) and (40) are the HTF matrices of the system, and are 6 x 6. In reality, when an LTP system is represented in the frequency domain, the HTF matrix has an infinite order [14]. In here, the HTF matrix is 6 x 6 because only the first round of couplings is considered. $M_{\text{LTP1+}}$ could be 2 x 2 if the couplings are ignored (considering $\overrightarrow{TF_{\text{PLL3+}}}$–$\overrightarrow{TF_{\text{PLL6+}}}$ negligible). Alternatively, $M_{\text{LTP1+}}$ could be higher order than 6 x 6 if the second or more rounds of couplings are considered. A question arises as to what is the appropriate order to model. The issue of model truncation is explained subsequently.

Formally, the poles of an LTP system are the locations in the complex s-plane where the HTF is not analytic [30]. According to [30], the LTP poles appear in different strips. The horizontal strip confined by $y = \omega_p/2$ and $y = -\omega_p/2$ (with ω_p being the pumping frequency of the LTP system; i.e. $4\omega_1$ in M1 and $2\omega_1$ in M2) is called the fundamental strip. The poles that appear in this strip are then reflected to other strips (i.e. complementary strips) in such a way that only the imaginary part of the poles change, but not the real part. This is illustrated in Fig. 11. This means that there are infinite LTP poles, but since the x-axis value of the poles does not change when comparing different strips, it is not necessary to look at all the poles of the system in order to assess stability, but only

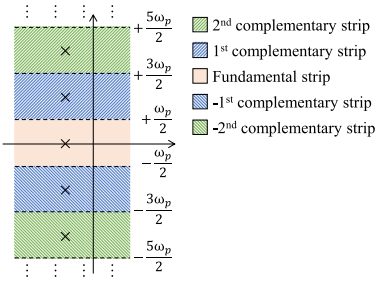

FIGURE 11. Infinite pole repetition in an LTP system [30].

whether the poles in the fundamental strip fall entirely in the LHP or not.

In this article, it is considered that a certain HTF order is enough as long as the poles in the fundamental strip do not significantly change. In practice, this means that the conclusions of the stability study (the stability limit) remain unchanged if the order is increased. As it will be shown later, the $M_{\text{LTP1+}}$ 2 x 2 HTF matrix predicts the same poles in the fundamental strip (and thus, the same stability limits) as the $M_{\text{LTP1+}}$ 6 x 6 HTF matrix. Since the LTP model is approximated as an LTI MIMO model of a certain order, the poles can be determined in the same way as with MIMO LTI theory [31].[6]

For method 2, the LTI and LTP MIMO matrices can be found similarly, leading to $M_{\text{LTI2+}}$, $M_{\text{LTI2-}}$, $M_{\text{LTP2+}}$ and $M_{\text{LTP2-}}$. In M2, however, it is only necessary to check the poles of the positive-sequence sub-system, since only $\theta_{\text{PLL+}}$ is fed back.

C. STABILITY RESULTS: METHOD 1

In this section, the parameter K that defines the cut-off frequency of the low-pass filter $F(s) = \frac{\omega_f}{s+\omega_f}$ (with $\omega_f = K\omega_1$) is changed. According to simulations, the DDSRF-PLL method 1 becomes unstable for K values higher than K_{lim}, being:

- $K_{\text{lim}} = 1.05$ for $V_n = 5\%$.
- $K_{\text{lim}} = 1.05$ for $V_n = 40\%$.

In Fig. 12 the pole maps[7] from $M_{\text{LTI1+}}$ and $M_{\text{LTI1-}}$ are shown for different K when $V_n = 5\%$. As it can be seen, the LTI method predicts incorrectly the stability boundary, since it predicts that, for $K = 1.15$ and $K = 1.35$, the system is still stable. The K has to be increased until $K = 2.45$ in order to predict instability (not shown in the figure). The pole maps of $M_{\text{LTP1+}}$ and $M_{\text{LTP1-}}$ are also shown in Fig. 12, and they

[6]This means that the same method for pole determination will be used for the LTP system as for the LTI system, which is to plot the poles of each individual transfer function in the matrix. This method is also used in [32].

[7]Only the poles close to the $x = 0$ line are shown.

$$\begin{bmatrix} \overrightarrow{TF_{\text{PLL1+}}(s)} & \overrightarrow{TF_{\text{PLL2+}}(s)} & \overrightarrow{TF_{\text{PLL3+}}(s)} & \overrightarrow{TF_{\text{PLL4+}}(s)} & \overrightarrow{TF_{\text{PLL5+}}(s)} & \overrightarrow{TF_{\text{PLL6+}}(s)} \\ \overrightarrow{TF^*_{\text{PLL2+}}(s)} & \overrightarrow{TF^*_{\text{PLL1+}}(s)} & \overrightarrow{TF^*_{\text{PLL4+}}(s)} & \overrightarrow{TF^*_{\text{PLL3+}}(s)} & \overrightarrow{TF^*_{\text{PLL6+}}(s)} & \overrightarrow{TF^*_{\text{PLL5+}}(s)} \\ \overrightarrow{TF_{\text{PLL5+}}(s-j4\omega_1)} & \overrightarrow{TF_{\text{PLL4+}}(s-j4\omega_1)} & \overrightarrow{TF_{\text{PLL1+}}(s-j4\omega_1)} & 0 & 0 & \overrightarrow{TF_{\text{PLL2+}}(s-j4\omega_1)} \\ \overrightarrow{TF^*_{\text{PLL4+}}(s+j4\omega_1)} & \overrightarrow{TF^*_{\text{PLL5+}}(s+j4\omega_1)} & 0 & \overrightarrow{TF^*_{\text{PLL1+}}(s+j4\omega_1)} & \overrightarrow{TF^*_{\text{PLL2+}}(s+j4\omega_1)} & 0 \\ \overrightarrow{TF_{\text{PLL3+}}(s+j4\omega_1)} & \overrightarrow{TF_{\text{PLL6+}}(s+j4\omega_1)} & 0 & \overrightarrow{TF_{\text{PLL2+}}(s+j4\omega_1)} & \overrightarrow{TF_{\text{PLL1+}}(s+j4\omega_1)} & 0 \\ \overrightarrow{TF^*_{\text{PLL6+}}(s-j4\omega_1)} & \overrightarrow{TF^*_{\text{PLL3+}}(s-j4\omega_1)} & \overrightarrow{TF^*_{\text{PLL2+}}(s-j4\omega_1)} & 0 & 0 & \overrightarrow{TF^*_{\text{PLL1+}}(s-j4\omega_1)} \end{bmatrix} \tag{41}$$

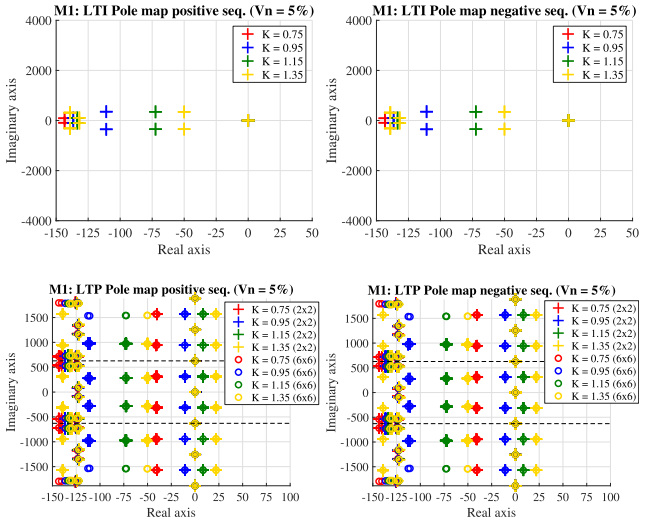

FIGURE 12. Stability results for method 1 ($V_n = 5\%$). The LTP pole map shows the fundamental strip, and two complementary strips (*y*-axis: $[\frac{-3\omega_p}{2} \frac{3\omega_p}{2}]$ with $\omega_p = 4\omega_1$).

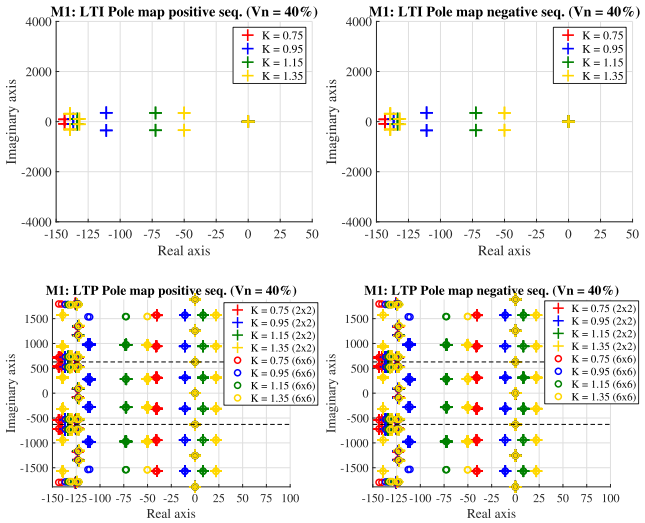

FIGURE 13. Stability results for method 1 ($V_n = 40\%$). The LTP pole map shows the fundamental strip, and two complementary strips (*y*-axis: $[\frac{-3\omega_p}{2} \frac{3\omega_p}{2}]$ with $\omega_p = 4\omega_1$).

correctly predict the stability boundary. Note that, no matter that the 2 x 2 or 6 x 6 LTP model is used, the stability limit is predicted accurately. In Fig. 13 the pole maps are shown for $V_n = 40\%$. Again, the stability prediction of the LTI model is incorrect, whereas the LTP models are accurate.

D. STABILITY RESULTS: METHOD 2

Here, K is also changed. According to simulations, the method 2 becomes unstable for K values higher than K_{lim}, being:

- $K_{lim} = 2.427$ for $V_n = 5\%$.
- $K_{lim} = 2.089$ for $V_n = 40\%$.

In Fig. 14 the pole map from M_{LTI2+} is shown for different K when $V_n = 5\%$. Note that, in method 2, it is only necessary to check the poles of the positive-sequence sub-system, since

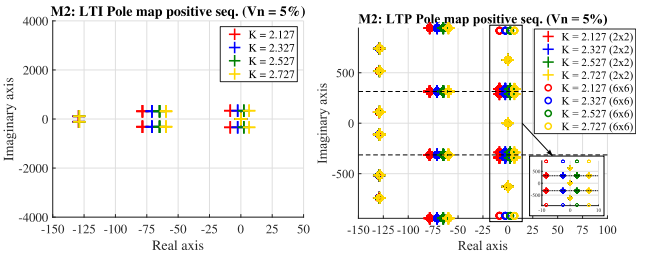

FIGURE 14. Stability results for method 2 ($V_n = 5\%$). The LTP pole map shows the fundamental strip, and two complementary strips (*y*-axis: $[\frac{-3\omega_p}{2} \frac{3\omega_p}{2}]$ with $\omega_p = 2\omega_1$).

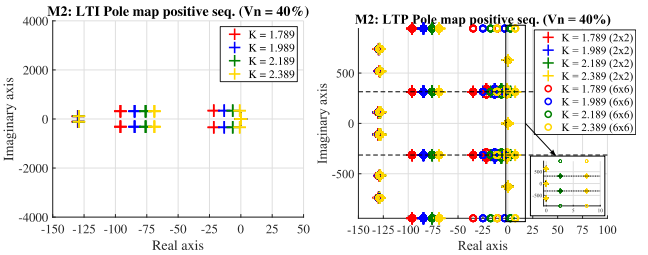

FIGURE 15. Stability results for method 2 ($V_n = 40\%$). The LTP pole map shows the fundamental strip, and two complementary strips (*y*-axis: $[\frac{-3\omega_p}{2} \frac{3\omega_p}{2}]$ with $\omega_p = 2\omega_1$).

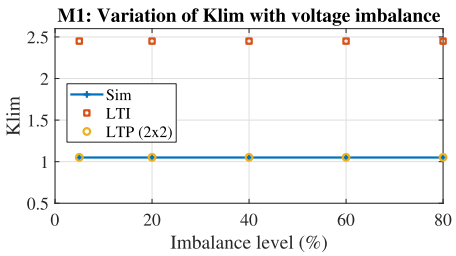

FIGURE 16. Method 1: variation of K_{lim} with voltage imbalance given by simulations, the LTI model and the LTP (2x2) model.

only θ_{PLL+} is used in the decoupling network. As it can be seen, the LTI method predicts quite accurately the stability boundary, since it predicts that, for the two K values higher than K_{lim}, the system is unstable. In contrast, when $V_n = 40\%$, the LTI model becomes inaccurate (Fig. 15). The LTP models (2x2 or 6x6) are accurate no matter the V_n level.

E. EXPLANATION OF THE STABILITY RESULTS

The results in relation to method 1 are explained first. In M1, it is important to look at the expressions (4) and (5). The periodic terms in (5) depend on V_p and, thus, the periodic terms are important even if V_n is low. Since the LTI model ignores all periodic terms, the stability of the network is wrongly predicted by the LTI model (see again Fig. 12 and Fig. 13). In contrast, the LTP model considers the periodic terms, and predicts stability accurately for all V_n levels. This is clearly shown in Fig. 16.

Thus, the periodic terms explain the inaccuracy of the LTI model shown in Fig. 16. Other issues to explain in this figure

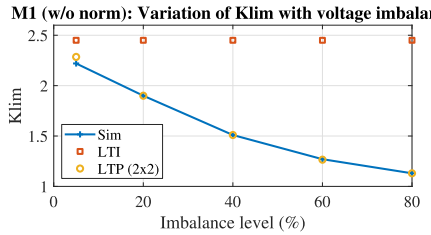

FIGURE 17. Method 1 (w/o normalization): variation of K_{lim} with voltage imbalance given by simulations, the LTI model and the LTP (2x2) model.

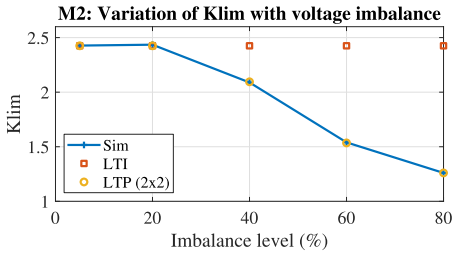

FIGURE 18. Method 2: variation of K_{lim} with voltage imbalance given by simulations, the LTI model and the LTP (2x2) model.

are: a) why the stability limit is independent on V_{n} (i.e. why K_{lim} is fixed at 1.05); and b) why the prediction of the LTI model is constant. The first issue is due to the normalization block. Including the normalization block makes the dynamics to be independent on V_{n}. In fact, the pole maps of the PLL do not change when V_{n} increases (compare the pole maps shown in Fig. 12 and Fig. 13). In contrast, if the normalization block is excluded, Fig. 17 is obtained. It is seen here that, in this case, K_{lim} depends on V_{n}. Here, note that the LTI model is also always inaccurate, although it is more inaccurate when V_{n} is high.

The second issue is why the stability prediction of the LTI model for method 1 is independent of V_{n}. The $\overrightarrow{TF_{\text{PLL1+LTI}}}$ in (24) does not depend on V_{n} and thus its poles (and the poles of $M_{\text{LTI1+}}$) do not change with V_{n}. With respect to $\overrightarrow{TF_{\text{PLL1–LTI}}}$, when the normalization block is included, then $\overrightarrow{TF_{\text{PLL1–LTI}}}$ becomes:

$$\overrightarrow{TF_{\text{PLL1–LTI}}} = \frac{V_{\text{nom}}}{V_{\text{n}}} \frac{H_{\text{PLL–}}(s)\overrightarrow{G^{*}_{\text{dq+}}(s)}}{2j(1 + V_{\text{nom}} H_{\text{PLL–}}(s) G_{\text{re}}(s))}. \quad (42)$$

V_{n} appears in (42) but only as a gain that cannot modify the poles of the system. Consequently, the LTI model in Fig. 16 always predicts a constant stability limit.

With respect to method 2, only $\theta_{\text{PLL+}}$ is used in the decoupling network. Therefore, the relevant periodic terms in order to determine the stability of the network are those which appear in (25) but not the ones which appear in (26). It can be seen that the periodic terms in (25) are low when V_{n} is low, and therefore, in the low-V_{n} cases the LTI model is accurate for stability calculations (see Fig. 14). When V_{n} increases, however, the periodic terms become relevant and again the LTI model fails to predict the stability boundary (see Fig. 15).

This is summarized in Fig. 18. In here, K_{lim} reduces with V_{n}, and the LTP model perfectly predicts the trend. The LTI model, however, is accurate only when V_{n} is low. Also, the LTI model predicts a constant $K_{\text{lim}} = 2.45$, independent of V_{n}. Of course, this is the case for the LTI model, since in M2 only the $M_{\text{LTI1+}}$ matters for stability and the $\overrightarrow{TF_{\text{PLL1+LTI}}}$ does not depend on V_{n}.

F. LTP MODEL ORDER TRUNCATION

Sections IX-C and IX-D show, both in M1 and M2, that the LTP poles in the fundamental strip do not significantly change when they are calculated with the 2 x 2 or 6 x 6 model. With respect to the other strips, the 6x6 model calculates more poles there, which is expected since the 6 x 6 model has a higher order. However, since the poles in the complementary strips are only reflections of the poles in the fundamental strip, only the poles in the fundamental strip are relevant for stability, and thus the 2 x 2 model is considered enough for stability studies. In fact, Fig. 16 – 18 show that the 2 x 2 model calculates the stability boundaries accurately; while Fig. 10 shows that the $\overrightarrow{TF_{\text{PLL1+}}}$ and $\overrightarrow{TF_{\text{PLL2+}}}$ alone predict the most relevant oscillations in the PLL response.

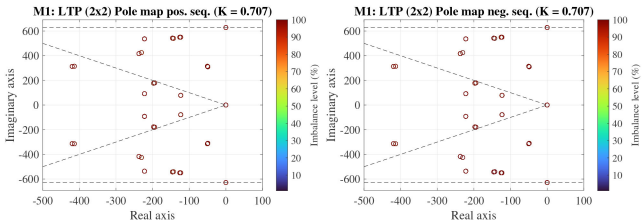

FIGURE 19. Method 1: pole map at different imbalance levels ($K = 1/\sqrt{2}$). The pole map shows the fundamental strip (y-axis: $[\frac{-\omega_{\text{p}}}{2} \frac{\omega_{\text{p}}}{2}]$ with $\omega_{\text{p}} = 2\omega_1$) and the $\zeta = 1/\sqrt{2}$ damping diagonals.

X. EXAMPLE OF APPLICATION OF THE LTP MODEL

The LTP model has been used to check the stability boundary. However, it can also provide further information, as for example, the stability margin of the PLL. An example of such usage is shown in this section.

The positive- and negative-sequence pole maps of method 1 when $K = 1/\sqrt{2}$ are shown in Fig. 19. First of all, it is noticeable that the pole map of method 1 (M1) does not change with V_{n}. This is due to the normalization block. If the normalization block is bypassed (in such a way that $v^{\text{dec}}_{\text{q–}}$ is directly fed into the PI), the polemaps vary with V_{n}, as shown in Fig. 20.

Fig. 21 shows the eigenvalue plot of method 2, which moves closer to $x = 0$ as the imbalance level increases. If ensuring a minimum level of damping as $\zeta = 1/\sqrt{2}$ is a requirement for the PLL design, it can be seen here that this parameter selection would only meet the requirement for low imbalance levels (in particular, for $V_{\text{n}} < 15$ %).

Another example would be to compare PLL types. In recent literature, the comparison of the response of different PLL

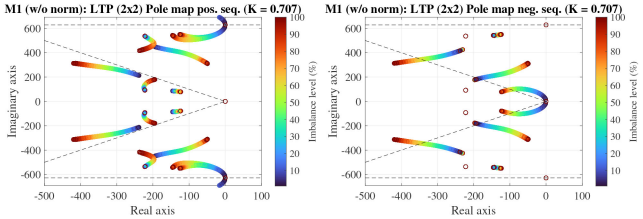

FIGURE 20. Method 1 (w/o norm): pole map at different imbalance levels ($K = 1/\sqrt{2}$). The pole map shows the fundamental strip (y-axis: $[\frac{-\omega_p}{2}\ \frac{\omega_p}{2}]$ with $\omega_p = 2\omega_1$) and the $\zeta = 1/\sqrt{2}$ damping diagonals.

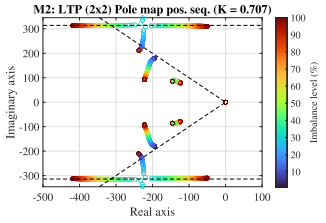

FIGURE 21. Method 2: pole map at different imbalance levels ($K = 1/\sqrt{2}$). The pole map shows the fundamental strip (y-axis: $[\frac{-\omega_p}{2}\ \frac{\omega_p}{2}]$ with $\omega_p = \omega_1$) and the $\zeta = 1/\sqrt{2}$ damping diagonals.

TABLE 1. Model Selection Recommendation Depending on the PLL Type and Voltage Imbalance Level

	Direct tracking of negative-sequence					Indirect tracking or no tracking of negative-sequence				
Imb. level	5%	20%	40%	60%	80%	5%	20%	40%	60%	80%
LTI						x	x			
LTP	x	x	x	x	x			x	x	x

topologies against faults has typically been done by comparing time domain waveforms, which leads to a comparison difficult to quantify. The presented LTP model can potentially be used as an additional tool to time domain simulations to compare different PLL topologies in a more quantitative way.

XI. GUIDELINES FOR LTI VS LTP MODEL SELECTION IN THE PRESENCE OF IMBALANCE

This article shows that the LTI model might provide inaccurate stability predictions depending on the V_n level and the way in which the negative-sequence voltage is tracked, while the LTP model calculates the stability boundary more accurately no matter the imbalance level nor the PLL method. Based on the results of this article, some conclusions can be generalized as basic guidelines for LTI vs LTP model selection for studying stability in PLLs. These conclusions are shown in Table 1.

Table 1 shows that, whenever the PLL indirectly tracks the negative-sequence voltage, for low levels of imbalance the LTI model can be used. In this article it has been shown that, for the DDSRF-PLL method 2, the LTI model gives results with high accuracy until $V_n = 20\%$ approximately, while for $V_n = 40\%$ and above the LTP model accuracy is much higher (see Fig. 18). It is clear that, for this specific PLL and for the exact parameter selection, the model-validity boundary for choosing the LTI model vs the LTP model is between $V_n = 20\%$ and $V_n = 40\%$. For other types of PLLs and parameters, this boundary might differ. It is worth to note that an imbalance level in between $20 - 40\%$ is a relatively high imbalance level that encompasses, to the knowledge of the authors, the imbalance levels that appear in normal operation conditions, and even some mild faulty conditions. It seems reasonable to assume, then, that for other types of PLLs, accurate results can be obtained with the LTI model if the analysis is performed in normal operating conditions, while if the analysis is performed for faulty conditions, the LTP model is probably necessary; although further investigations with other PLL topologies are recommended. In the case in which the negative-sequence is not tracked (which is M2 without the extra blocks to calculate the negative sequence characteristics), this boundary of $V_n = 20 - 40\%$ will be applicable, since in method 2 the stability depends only on tracking the positive-sequence phase angle. In the case that the negative-sequence voltage is directly tracked, it is always necessary to use an LTP model, since the periodicity in the state variables is brought forward by both V_p and V_n.

It could be argued, then, that the LTP model should always be used, especially if the model-validity boundary between using the LTI and LTP model is unknown. However, this ignores one main drawback of the LTP method, which is its higher computational effort with respect to the LTI model.[8] Therefore, the final selection can be performed taking into account the computational efficiency as well, although always taking into account the accuracy considerations shown in Table 1.

XII. CONCLUSION

The LTI and LTP models of two different DDSRF-PLL methods in the presence of voltage imbalance have been derived. The article shows that, when the PLL directly tracks the negative-sequence phase-angle (method 1), the LTP terms depend on both V_p and V_n, separately. Thus, even if the voltage imbalance is low, the LTP dynamics are relevant and influence the stability of the PLL (due to V_p). The main consequence is that the LTI model cannot predict correctly the stability limit at any imbalance level. In contrast, when the PLL indirectly tracks the negative-sequence phase-angle (method 2), the LTP terms depend on V_n only. Thus, when V_n is low enough (with respect to V_p) the LTI model predicts correctly the stability boundaries, although when V_n is increased, the LTP model is needed. Some guidelines as to how to pick between LTI and LTP models for stability analysis of DDSRF-PLLs in the presence of imbalance have been given.

Further, the article shows with time domain simulations that, in order to capture the most relevant oscillations that

[8] It is worth to note, however, that the computational effort of the LTP model highly depends on the type of LTP model used. This article uses a closed-loop HTF, although other LTP modelling alternatives are possible, like using open-loop HTFs (e.g. [11]) or using the time domain state-space approach (e.g. [13]), which are more computationally efficient than the closed-loop HTF approach.

occur in the PLL in the presence of V_n, it is not necessary to include the coupling terms in the LTP model. In fact, it is shown that a 2x2 HTF matrix is enough for predicting the stability limit, although the order can always be increased to enhance accuracy.

APPENDIX A
DESIGN OF DDSRF-PLL CONSTANTS

This Appendix discusses the DDSRF-PLL constants. The first design choice is the cut-off frequency of: $F(s) = \frac{\omega_f}{s+\omega_f}$. This frequency is usually set as $\omega_f = K\omega_1$, where K is the parameter changed in Section IX to test the LTI and LTP methods. The second design choice is the constants in the PI regulators. In this article, the same strategy as in [2] is followed, which consists in ignoring the decoupling network and analysing the SRF-PLL separately. In this case, the SRF-PLL is a second-order small-signal model with two poles whose locations depend on K_{pPLL} and K_{iPLL}. The damping and frequency of the poles can be imposed (in this article, $\omega_c = 2\pi 30$ rad/s and $\xi = 1/\sqrt{2}$) as:

$$K_{iPLL} = \frac{\omega_c^2}{V_{nom}}\ ;\ K_{pPLL} = \frac{2\xi\omega_c}{V_{nom}} \tag{43}$$

where V_{nom} is the nominal converter voltage (in this article, $V_{nom} = 110\sqrt{2}$ V). These PI values are used in the positive-sequence SRF-PLL in both methods. In the negative-sequence SRF in method 1, these constants are used too, since the negative-sequence voltage is normalized and scaled to V_{nom}.

APPENDIX B
EXTRA EQUATIONS FOR LTP MODEL OF METHOD 1

A generic term $\overrightarrow{T}$ is defined as $\overrightarrow{T} = \overrightarrow{T_0(s + j2\omega_1)}$ (with $\overrightarrow{T_0}$ defined in (11)) and:

$$\begin{aligned}
\overrightarrow{T_1} &= \overrightarrow{G_{dq+}(s)}\left(1 - jV_n\overrightarrow{G^*_{dq+}(s + j2\omega_1)}\overrightarrow{T}\right)\\
\overrightarrow{T_2} &= -jV_p\overrightarrow{T_1}\\
\overrightarrow{T_3} &= jV_n e^{-2j(\phi_{vp}+\phi_{vn})}\overrightarrow{G_{dq+}(s)}\overrightarrow{G_{dq+}(s + j2\omega_1)}\overrightarrow{T}\\
\overrightarrow{T_4} &= jV_p\overrightarrow{T_3}\\
\overrightarrow{T_5} &= \frac{H_{PLL+}(s)}{2j - H_{PLL+}(s)(\overrightarrow{T_2} - \overrightarrow{T_2^*})}.
\end{aligned} \tag{44}$$

APPENDIX C
EXTRA EQUATIONS FOR LTP MODEL OF METHOD 2

$$\begin{aligned}
\overrightarrow{T_6} &= \frac{H_{PLL+}(s)}{2j(1 + V_p H_{PLL+}(s)G_{re}(s))}\\
\overrightarrow{T_7} &= jV_n e^{j(\phi_{vp}+\phi_{vn})}\overrightarrow{G^*_{dq+}(s)}
\end{aligned} \tag{45}$$

REFERENCES

[1] S. Golestan, J. M. Guerrero, and J. C. Vasquez, "Three-phase PLLs: A review of recent advances," *IEEE Trans. Power Electron.*, vol. 32, no. 3, pp. 1894–1907, Mar. 2017, doi: 10.1109/TPEL.2016.2565642.

[2] P. Rodriguez, J. Pou, J. Bergas, J. I. Candela, R. P. Burgos, and D. Boroyevich, "Decoupled double synchronous reference frame PLL for power converters control," *IEEE Trans. Power Electron.*, vol. 22, no. 2, pp. 584–592, Mar. 2007.

[3] Ö. C. Sakinci and J. Beerten, "Comparison of linear time-invariant and linear time-periodic models for small-signal stability analysis of power electronic converters," in *Proc. Young Researchers Symp.*, 2018, pp. 1–5.

[4] Ö. C. Sakinci and J. Beerten, "Equivalent multiple dq-frame model of the MMC using dynamic phasor theory in the $\alpha\beta z$-frame," *IEEE Trans. Power Del.*, vol. 35, no. 6, pp. 2916–2927, Dec. 2020, doi: 10.1109/TPWRD.2020.3025388.

[5] S. Golestan, J. M. Guerrero, and J. C. Vasquez, "LTP modeling of single-phase $t/4$ delay-based PLLs," *IEEE Trans. Ind. Electron.*, vol. 68, no. 9, pp. 9003–9008, Sep. 2021, doi: 10.1109/TIE.2020.3018046.

[6] S. Golestan, J. M. Guerrero, and J. C. Vasquez, "Modeling and stability assessment of single-phase grid synchronization techniques: Linear time-periodic versus linear time-invariant frameworks," *IEEE Trans. Power Electron.*, vol. 34, no. 1, pp. 20–27, Jan. 2019, doi: 10.1109/TPEL.2018.2835144.

[7] S. Golestan, J. M. Guerrero, J. C. Vasquez, A. M. Abusorrah, and Y. Al-Turki, "Standard SOGI-FLL and its close variants: Precise modeling in LTP framework and determining stability region/robustness metrics," *IEEE Trans. Power Electron.*, vol. 36, no. 1, pp. 409–422, Jan. 2021, doi: 10.1109/TPEL.2020.2997603.

[8] S. Wang, Z. Yuan, J. Ma, T. Liu, Z. Wu, and R. Wang, "Accurate LTP model and stability analysis of the second-order generalized integrator-based single-phase phase-locked loop," *IEEE Trans. Ind. Electron.*, vol. 69, no. 6, pp. 6225–6235, Jun. 2022, doi: 10.1109/TIE.2021.3090699.

[9] C. Zhang, S. Føyen, J. A. Suul, and M. Molinas, "Modeling and analysis of SOGI-PLL/FLL-based synchronization units: Stability impacts of different frequency-feedback paths," *IEEE Trans. Energy Convers.*, vol. 36, no. 3, pp. 2047–2058, Sep. 2021, doi: 10.1109/TEC.2020.3041797.

[10] S. Shah, P. Koralewicz, V. Gevorgian, and L. Parsa, "Small-signal modeling and design of phase-locked loops using harmonic signal-flow graphs," *IEEE Trans. Energy Convers.*, vol. 35, no. 2, pp. 600–610, Jun. 2020, doi: 10.1109/TEC.2019.2954112.

[11] S. Golestan, J. M. Guerrero, J. C. Vasquez, A. M. Abusorrah, and Y. Al-Turki, "Linear time-periodic modeling, examination, and performance enhancement of grid synchronization systems with DC component rejection/estimation capability," *IEEE Trans. Power Electron.*, vol. 36, no. 4, pp. 4237–4253, Apr. 2021, doi: 10.1109/TPEL.2020.3018584.

[12] Y. Liao, X. Wang, X. Yue, and H. Gong, "Harmonic transfer-function model of three-phase synchronous reference frame PLL under unbalanced grid conditions," in *Proc. IEEE Appl. Power Electron. Conf. Expo.*, 2019, pp. 58–65, doi: 10.1109/APEC.2019.8721842.

[13] P. D. Achlerkar and B. K. Panigrahi, "New perspectives on stability of decoupled double synchronous reference frame PLL," *IEEE Trans. Power Electron.*, vol. 37, no. 1, pp. 285–302, Jan. 2022, doi: 10.1109/TPEL.2021.3099162.

[14] S. R. Hall and N. M. Wereley, "Generalized nyquist stability criterion for linear time periodic systems," in *Proc. Amer. Control Conf.*, 1990, pp. 1518–1525, doi: 10.23919/ACC.1990.4790991.

[15] F. D. Freijedo, J. Doval-Gandoy, O. Lopez, and E. Acha, "Tuning of phase-locked loops for power converters under distorted utility conditions," *IEEE Trans. Ind. Appl.*, vol. 45, no. 6, pp. 2039–2047, Nov./Dec. 2009, doi: 10.1109/TIA.2009.2031790.

[16] S. Golestan, M. Ramezani, J. M. Guerrero, F. D. Freijedo, and M. Monfared, "Moving average filter based phase-locked loops: Performance analysis and design guidelines," *IEEE Trans. Power Electron.*, vol. 29, no. 6, pp. 2750–2763, Jun. 2014, doi: 10.1109/TPEL.2013.2273461.

[17] H. Awad, J. Svensson, and M. Bollen, "Tuning software phase-locked loop for series-connected converters," *IEEE Trans. Power Del.*, vol. 20, no. 1, pp. 300–308, Jan. 2005, doi: 10.1109/TPWRD.2004.837823.

[18] P. Rodríguez, R. Teodorescu, I. Candela, A. V. Timbus, M. Liserre, and F. Blaabjerg, "New positive-sequence voltage detector for grid synchronization of power converters under faulty grid conditions," in *Proc. 37th IEEE Power Electron. Specialists Conf.*, 2006, pp. 1–7, doi: 10.1109/pesc.2006.1712059.

[19] M. Karimi-Ghartemani and M. Iravani, "A method for synchronization of power electronic converters in polluted and variable-frequency environments," *IEEE Trans. Power Syst.*, vol. 19, no. 3, pp. 1263–1270, Aug. 2004, doi: 10.1109/TPWRS.2004.831280.
[20] D. Yazdani, M. Mojiri, A. Bakhshai, and G. Joós, "A fast and accurate synchronization technique for extraction of symmetrical components," *IEEE Trans. Power Electron.*, vol. 24, no. 3, pp. 674–684, Mar. 2009, doi: 10.1109/TPEL.2008.2010321.
[21] M. Karimi-Ghartemani and H. Karimi, "Processing of symmetrical components in time-domain," *IEEE Trans. Power Syst.*, vol. 22, no. 2, pp. 572–579, May 2007.
[22] A. Luna *et al.*, "Grid voltage synchronization for distributed generation systems under grid fault conditions," *IEEE Trans. Ind. Appl.*, vol. 51, no. 4, pp. 3414–3425, Jul./Aug. 2015, doi: 10.1109/TIA.2015.2391436.
[23] M. Karimi-Ghartemani, B.-T. Ooi, and A. Bakhshai, "Application of enhanced phase-locked loop system to the computation of synchrophasors," *IEEE Trans. Power Del.*, vol. 26, no. 1, pp. 22–32, Jan. 2011, doi: 10.1109/TPWRD.2010.2064341.
[24] L. Beloqui Larumbe, Z. Qin, L. Wang, and P. Bauer, "Impedance modelling for three-phase inverters with double synchronous reference frame current controller in the presence of imbalance," *IEEE Trans. Power Electron.*, vol. 37, no. 2, pp. 1461–1475, Feb. 2022, doi: 10.1109/TPEL.2021.3107045.
[25] L. Beloqui Larumbe, Z. Qin, and P. Bauer, "On the importance of tracking the negative-sequence phase-angle in three-phase inverters with double synchronous reference frame current control," in *Proc. 29th IEEE Int. Symp. Ind. Electron.*, 2019, pp. 1284–1289.
[26] P. Achlerkar and B. K. Panigrahi, "Dynamic harmonic domain modeling and stability augmented design of inverter interface to weak and unbalanced grid," *IEEE Trans. Power Del.*, doi: 10.1109/TPWRD.2021.3123370.
[27] J. Zhu, J. Hu, S. Wang, and M. Wan, "Small-signal modeling and analysis of MMC under unbalanced grid conditions based on linear time-periodic (LTP) method," *IEEE Trans. Power Del.*, vol. 36, no. 1, pp. 205–214, Feb. 2021, doi: 10.1109/TPWRD.2020.2976776.
[28] L. Harnefors, "Modeling of three-phase dynamic systems using complex transfer functions and transfer matrices," *IEEE Trans. Ind. Electron.*, vol. 54, no. 4, pp. 2239–2248, Aug. 2007, doi: 10.1109/TIE.2007.894769.
[29] J. M. Maciejowski, *Multivariable Feedback Design*. Reading, MA, USA: Addison Wesley, 1989.
[30] N. M. Wereley and S. R. Hall, "Linear time periodic systems: Transfer function, poles, transmission zeroes and directional properties," in *Proc. Amer. Control Conf.*, 1991, pp. 1179–1184, doi: 10.23919/ACC.1991.4791563.
[31] E. Mollerstedt and B. Bernhardsson, "Out of control because of harmonics-an analysis of the harmonic response of an inverter locomotive," *IEEE Control Syst.*, vol. 20, no. 4, pp. 70–81, Aug. 2000.
[32] J. Lyu, X. Cai, X. Zhang, and M. Molinas, "Harmonic state space modeling and analysis of modular multilevel converter," in *Proc. IEEE Int. Power Electron. Appl. Conf. Expo.*, 2018, pp. 1–6, doi: 10.1109/PEAC.2018.8590305.

LUCIA BELOQUI LARUMBE (Student Member, IEEE) was born in Pamplona, Spain, in 1993. She received the B.Sc. and M.Sc. degrees in electrical engineering from the Public University of Navarre, Pamplona, Spain, in 2015 and 2017, respectively, where she is currently pursuing a Ph.D. degree with the Delft University of Technology, Delft, The Netherlands. She did her Master's thesis with the Delft University of Technology on the topic of advanced control for microgrids. In 2017, she joined the DC systems, Energy Conversion and Storage Group, Delft University of Technology. Her research interests include control of power electronics, power quality, stability, and renewable energies.

ZIAN QIN (Senior Member, IEEE) received the B.Eng. degree in automation from Beihang University, Beijing, China, in 2009, the M.Eng. degree in control science and engineering from the Beijing Institute of Technology, Beijing, China, in 2012, and the Ph.D. degree from Aalborg University, Aalborg, Denmark, in 2015. He is currently an Assistant Professor with the Delft University of Technology, Delft, The Netherlands. In 2014, he was a Visiting Scientist with Aachen University, Aachen, Germany. From 2015 to 2017, he was a Postdoctoral Research Fellow with Aalborg University. He has authored or coauthored more than 90 journals/conference articles, four book chapters, and two international patents in his research areas, which include power quality and stability of power electronics-based grid, and solid state transformers. He has also worked on several European and Dutch national projects regarding the power quality of wind farms and EV charging. He is leading the research on solid-state transformers in FlexH2. He is an Associate Editor for IEEE TRANSACTIONS ON INDUSTRIAL ELECTRONICS, and the Guest Associate Editor of IEEE JOURNAL OF EMERGING AND SELECTED TOPICS, and IEEE TRANSACTIONS ON ENERGY CONVERSION. He is a Distinguished Reviewer for 2020 of IEEE TRANSACTIONS OF INDUSTRIAL ELECTRONICS. He was the Technical Program Chair of IEEE-ISIE 2020, Technical Program Co-Chair of IEEE-COMPEL 2020, Industrial Session Co-Chair of ECCE-Asia 2020.

PAVOL BAUER (Senior Member, IEEE) received the master's degree in electrical engineering from the Technical University of Kosice, Kosice, Slovakia, in 1985, and the Ph.D. degree from the Delft University of Technology, Delft, The Netherlands, in 1995. He is currently a Full Professor with the Department of Electrical Sustainable Energy of Delft University of Technology, and the Head of DC Systems, Energy Conversion and Storage Group. He is also a Professor with the Brno University of Technology, Brno, Czech Republic, and an Honorary Professor with Politehnica University Timişoara, Timişoara, Romania. From 2002 to 2003, he was partially with KEMA (DNVGL, Arnhem) on different projects related to power electronics applications in power systems. He has authored or coauthored more than 120 journal and 500 conference articles in his research fields (with H factor Google scholar 40, Web of Science 26). He is the author or coauthor of eight books, holds seven international patents and organized several tutorials at the international conferences. His main research interests include power electronics for charging of electric vehicles and DC grids. He has worked on many projects for industry concerning wind and wave energy, power electronic applications for power systems, such as Smart-trafo and HVDC systems, projects for smart cities, such as PV charging of electric vehicles, PV and storage integration, contactless charging, and participated in several Leonardo da Vinci, H2020 and Electric Mobility Europe EU Projects as a Project partner (ELINA, INETELE, E-Pragmatic, Micact, Trolley 2.0, OSCD, P2P, Progressus) and a Coordinator (PEMCWebLab.com-Edipe, SustEner, Eranet DCMICRO). He is the former Chairman of Benelux IEEE Joint Industry Applications Society, Power Electronics and Power Engineering Society Chapter, Chairman of the Power Electronics and Motion Control Council, Member of the Executive Committee of European Power Electronics Association, and also Member of international steering committee at numerous conferences.